Hydrol. Earth Syst. Sci. Discuss., 12, 2011–2046, 2015
www.hydrol-earth-syst-sci-discuss.net/12/2011/2015/
doi:10.5194/hessd-12-2011-2015

Hydrology and Earth System Sciences Discussions

Open Access

Integration of 2-D hydraulic model and high-resolution LiDAR-derived DEM for floodplain flow modeling

D. Shen[1,2,3], J. Wang[1,2], X. Cheng[3], Y. Rui[1,2], and S. Ye[3]

[1]Jiangsu Provincial Key Laboratory of Geographic Information Science and Technology, Nanjing, Jiangsu, China
[2]Department of Geographic Information Science, Nanjing University, Nanjing, Jiangsu, China
[3]Changjiang River Scientific Research Institute, Changjiang Water Resources Commission, Wuhan, Hubei, China

Received: 22 January 2015 – Accepted: 1 February 2015 – Published: 13 February 2015

Correspondence to: J. Wang (wangjiechen@hotmail.com)

Published by Copernicus Publications on behalf of the European Geosciences Union.

Abstract

The rapid progress of Light Detection And Ranging (LiDAR) technology has made acquirement and application of high-resolution digital elevation model (DEM) data increasingly popular, especially with regards to the study of floodplain flow modeling. High-resolution DEM data include many redundant interpolation points, needs a high amount of calculation, and does not match the size of computational mesh. These disadvantages are a common problem for floodplain flow modeling studies. Two-dimensional (2-D) hydraulic modeling, a popular method of analyzing floodplain flow, offers high precision of elevation parameterization for computational mesh while ignoring much micro-topographic information of the DEM data itself. We offer a flood simulation method that integrates 2-D hydraulic model results and high-resolution DEM data, enabling the calculation of flood water levels in DEM grid cells through local inverse distance weighted interpolation. To get rid of the false inundation areas during interpolation, it employs the run-length encoding method to mark the inundated DEM grid cells and determine the real inundation areas through the run-length boundary tracing technique, which solves the complicated problem of the connectivity between DEM grid cells. We constructed a 2-D hydraulic model for the Gongshuangcha polder, a flood storage area of Dongting Lake, using our integrated method to simulate the floodplain flow. The results demonstrate that this method can solve DEM associated problems efficiently and simulate flooding processes with greater accuracy than DEM only simulations.

1 Introduction

Floodplain flow simulation is important for forecasting floods and assessing flood disasters. The typical focus of simulation studies is to predict accurate flood inundation extent, depth and duration (Garcia, 2004; Sanyal et al., 2006). In the field of hydraulic calculation, to build a one-dimensional (1-D) and two-dimensional (2-D) hydraulic mod-

HESSD

12, 2011–2046, 2015

els is a common method (Merwade et al., 2008). A 1-D hydraulic model is a traditional model, which usually simplifies hydraulic conditions and their physical processes, unable to show and simulate complicated river networks (Gichamo et al., 2012; Samuels, 1990). In comparison, a 2-D hydraulic model can simulate the floodplain condition in different periods and places, and calculate inundation extent and depth. Due to these advantages, 2-D models are commonly used in floodplain flow studies (Archambeau et al., 2004).

Digital elevation model (DEM) data is the most important data resource for floodplain flow models (Garrote et al., 1995). Its horizontal resolution and vertical elevation precision have much to do with the results calculated by 2-D hydraulic modeling (Bates et al., 1996). A few years ago, precise floodplain flow simulation, limited by the accuracy of the DEM data, was the bottleneck problem for 2-D hydraulic modeling (Apel et al., 2009). However, the increasing maturity of airborne Light Detection And Ranging (LiDAR) technology has made the acquirement and implement of high-resolution DEM data far easier in recent years. By processing the point cloud data, we can make the spatial resolution of DEM data 1 m and the vertical error 10–15 centimeters (Haile, 2005). With the high resolution, regional topographic information can be more detailed and micro-topography information of the flattened ditches and balks can be retained, offering the basis for more precise calculation of flood extent and depth (Horritt et al., 2001; Li et al., 2010; Merwade et al., 2008; French, 2003). Many scholars have tried to apply high-resolution LiDAR-derived DEM data to floodplain flow models and analyze the effects of different spatial DEM data resolution on model calculations (Sanders, 2007; Raber et al., 2007). Applying high-resolution DEM data to floodplain flow models has become a common trend in flood studies (Archambeau et al., 2004; Bates et al., 2000).

Although many studies claim that they have achieved satisfying results with the help of high-resolution DEM data, their methods still have weaknesses (Marks et al., 2000). In 2-D hydraulic models, topography is often represented by unstructured or structured mesh, and DEM data is used for the valuation assignments of computational mesh nodes. The denser a hydraulic model mesh is, the more time should be spent on the calculation process, which is limited by the processing ability of computers and the complexity of model. Due to high efficiency demands for model calculations, the mesh constructed by a hydraulic model is usually sparser than a DEM grid.

Under mid- or low-resolution DEM, topography appears flatter, allowing the DEM elevation change within a mesh element to be ignored, while hundreds of points of high-resolution LiDAR-derived DEM can keep much micro-topography information that is of high value in calculating inundation extent and depth (Schumann et al., 2008). If DEM data only serves for the valuation assignments of computational mesh nodes, then a lot of elevation point information is largely wasted (Marks et al., 2000). What's more, the quality of mesh resolution has little effect on the results of 2-D hydraulic models. Horritt et al. (2001) show that as the resolution of a computational mesh under the same DEM increases from 1000 to 10 m, the calculation result ceases to gain any additional precision once the resolution reaches 100 m. In applying 2-D hydraulic models to the floodplain flow, errors caused by precision differences between the collections of topography data are far greater than those caused by the differences between models (Fewtrell et al., 2011). Efficient processing of large amounts of DEM data and optimizing the precision of high-resolution vertical and horizontal information is the key to efficient and accurate analysis of large-scale automatic floodplain flow models.

As a result, we put forward a new flood simulation method that integrates a 2-D hydraulic model with high-resolution DEM data. Starting with high-resolution DEM data, we constructed a comparatively coarse computational mesh and then constructed a 2-D hydraulic model. The results of the 2-D hydraulic model were overlaid with the high-resolution DEM data and the flood depth in DEM grid cells was calculated using local inverse distance weighted interpolation. During the process of interpolation, there can be many false flood areas in the DEM grid because parts of the grid cells are interpolated despite not being inundated. To remove false-flooded areas, we marked all of the flooded areas using run-length encoding and then got the real flood extent through run-length boundary tracing technology, a method that proved to save much effort in

HESSD
12, 2011–2046, 2015

verifying the connectivity between DEM grid cells. Lastly, we constructed a 2-D hydraulic model for the Gongshuangcha polder, which is a flood storage area of Dongting Lake, and calculated the inundation extent and depth in different periods using our integrated method. By analyzing and comparing the results, it proves that this method can enhance the accuracy and reliability of floodplain flow modeling.

2 Study area and 2-D hydraulic model

2.1 Study area and DEM dataset

Dongting Lake (111°40′–113°10′ E, 28°30′–30°20′ N), with a total area of 18 780 km^2, is located in the middle reaches of Yangtze River (Changjiang River, Fig. 1). The districts through which the Dongting Lake flows include Changde, Yiyang, Yueyang, Changsha, Xiangtan, and Zhuzhou in Hunan Province as well as three cities in Jinzhou of Hubei Province. Dongting Lake is surrounded by mountains on three sides and its fountainheads are varied and complicated. It is a centripetal water system fanning out from the center. It only flows into the Yangtze River through Chenglingji of Yueyang (Fig. 1).

Because of its special location and complex river network system, this area has been frequently prone to flooding. Due to the heavy burden on the masses to deal with floods, lots of labor and money has been spent on dike construction. In order to prevent floods, a total of 266 levees have been built around Dongting Lake areas, and the total length of 5812 km with the first rank 3471 km and the second rank 1509 km. Flooding events in this area have caused significant destruction. The cost of damages following individual events in 1996 and 1998 was CNY 15 and 8.9 billion, respectively. The pressure of preventing flooding, and the associated damage, has been a major factor affecting healthy economic development and improvement of living standards in Hunan province.

Gongshuangcha polder, one of the largest flood storage zones in the Dongting Lake area, is located in the north of Yuanjiang county, facing South Dongting Lake to the

HESSD
12, 2011–2046, 2015

east and Chi Mountain to the west with water in between (Fig. 2). In total, the polder is 293 km^2 in storage area, 121.74 km in levee length, 33.65 m in storage height, has a storage volume of 1.85×10^9 m^3, and is home to 160 000 inhabitants.

We have employed the airborne laser-measuring instrument HARRIER 86i, from German TopoSys Company, for aerial photography of the Gongshuangcha polder since December 2010. The digital camera we used was a Trimble Rollei Metric AIC Pro and the inertial navigation system was Applanix POS/AV with a sampling frequency of 200 Hz. The laser scanner was Riegl LMS-Q680i, with a maximum pulse rate of 80–400 KHz and scanning angle of 45/60.

By processing the point cloud data, we derived a high-resolution DEM of the Gongshuangcha polder (Fig. 3). The spatial reference is the Gauss–Kruger projection coordinate system with Beijing 1954 datum, and the elevation system is based on the 1985 national elevation standard, of which the lowest elevation is 4.55 m and highest 45.87 m. The general landscape shown in the DEM is flat, with much micro topography information of levees, dikes and ridges retained (Fig. 3).

2.2 2-D hydraulic model

In 2008, the Changjiang Water Resources Commission approved a report on the Comprehensive Treatment Planning of Dongting Lake Area (Changjiang Water Resources Commission, 2008). The report highlighted the serious threat of floods, which cause a surplus water volume of $21.8–28 \times 10^9$ m^3, in the middle and lower reaches of Yangtze River. It also stressed that the effects of the Three Gorges Project, which greatly influences the conditions for incoming water and sediments, must be taken into consideration. Even though the completion of Three Gorges, and Xiluodu and Xiangjiaba Dams on the Chin-sha River can enhance the flood draining ability around Chenglingji (Fig. 1), at the confluence of Dongting Lake and Yangtze River, is the report emphasized the urgent need to construct a 10×10^9 m^3 of diversion storage zone around Chenglingji.

According to the Report on the Feasibility of the Flood Control Project of Qianliang Lake, Gongshuangcha and East Datong Lake of Dongting Lake Areas (Ministry of Water Resources of China, 2009), flood waters from events in 1954, 1966 and 1998, in Chenglingji could have been restricted to safely manageable levels if local polders were set up to divert 8000–12 000 $m^3 s^{-1}$ of rising waters. For the 1954 flood event, the report shows that the maximum diversion should have been set at 10 000 $m^3 s^{-1}$, with Qianliang Lake Polder contributing 4180 $m^3 s^{-1}$, Gongshuangcha Polder 3630 $m^3 s^{-1}$, and Datong Lake Polder 2190 $m^3 s^{-1}$, with the corresponding water levels for the dikes set at 33.06, 33.10 and 33.07 m.

According to the standard design of the Gongshuangcha Polder diversion, we simulated flood flow using a mode controlled by sluice behavior. The resulting hydrograph acted as the input parameter, with flood flow into the sluice conditioned as follows: when water level (H) was below 31.63 m, the flow volume into the sluice was 3630 $m^3 s^{-1}$; when H was 31.63–32.60 m, flow volume was 3050 $m^3 s^{-1}$; when H was 32.60–33.65 m, another flow diversion exit was opened.

The flood routing model employed 2-D unsteady shallow water equations to describe the water flow, used finite volume method (FVM) and Riemann approximate solvers to solve the coupled equations, and simulated flood routing inside the polder. We used non-structural discrete mesh to represent the computational zone based on the landscape of the area and the location of water conservancy projects. Then to make ensure accurate conservation, we used FVM to decide bulk, momentum and the equilibrium of density for each mesh element in different periods. To ensure precision, we used Riemann approximate solver to calculate the bulk and normal numerical flux of the momentum between the mesh elements. The model solves the equations through FVM discretions and converting 2-D problems into series of 1-D problems with the help of the coordinate rotation of fluxes. The basic principles are as follows.

1. Basic Control Equation. The Vector Expression of Conservative 2-D Shallow Water Equation:

$$\frac{\partial \boldsymbol{q}}{\partial t} + \frac{\partial \boldsymbol{f}(q)}{\partial x} + \frac{\partial \boldsymbol{g}(q)}{\partial y} = b(q) \quad (1)$$

HESSD
12, 2011–2046, 2015

In this expression the conservative vector $\boldsymbol{q} = [h, hu, hv]^{\mathrm{T}}$, the flux vector of X direction $\boldsymbol{f}(q) = [hu, hu^2 + gh^2/2, huv]^{\mathrm{T}}$, and the flux vector of Y direction $\boldsymbol{g}(q) = [hv, huv, hv^2 + gh^2/2]^{\mathrm{T}}$. h is height, u and v correspondingly mean the average uniform flux of X and Y directions, g is the gravity and the source term $b(q)$ is:

$$b(q) = [\boldsymbol{q}_{\mathrm{w}}, gh(s_{0x} - s_{fx}) + \boldsymbol{q}_{\mathrm{w}}u, gh(s_{0y} - s_{fy})] \quad (2)$$

In this expression, S_{0x} and S_{fx} are the river slope and friction slope on X direction; S_{0y} and S_{fy} are the river slope and friction slope on Y direction; $\boldsymbol{q}_{\mathrm{w}}$ is the net depth of water in each time unit. The friction slope could be calculated through Manning Formula.

2. The Discretization of Equations. Calculate basic FVM equation through discretization on any unit of Ω by divergence principle.

$$\iint_{\Omega} \boldsymbol{q}_t \mathrm{d}\varpi = -\int_{\partial\Omega} F(q) \cdot n \mathrm{d}L + \iint_{\Omega} b(q) \mathrm{d}\varpi \quad (3)$$

In this expression, n is the normal numerical flux outside of unit $\partial\Omega$, $\mathrm{d}\varpi$ and $\mathrm{d}L$ are surface integration and line integration, and $F(q)n$ is the normal numerical flux, where $F(q) = [\boldsymbol{f}(q), \boldsymbol{g}(q)]^{\mathrm{T}}$. These equations demonstrate that the solution could convert 2-D problems into series of local 1-D problems.

3. Boundary Condition. The model sets five kinds of flow boundaries: earth boundary, the outer boundary of slow and rushing flow, the inner boundary, flowing boundary of no-water and water exchange unit and tributary boundary of wetland.

4. The solution to the equation. The equations, which are explicit finite schemes can be solved through interactive method over time.

The computational mesh of the 2-D hydraulic model of Gongshuangcha Polder (Fig. 4) is constructed by a non-structural triangular mesh in which there are 83 378 triangles,

HESSD
12, 2011–2046, 2015

each of whose side length is between 100–150 m. The model mesh densifies the main levees with triangulars (each side length is between 60–80 m). With the 1 m-resolution DEM data, we get the elevation value of the mesh node and triangles centre points through nearest interpolation and make the value as the initial condition. The model computes the water level of each triangular mesh's central point every 10 min. Finally, it simulates 50 periods' inundation processes (8 h and 20 min in total).

3 Methodology

3.1 Overview

The inundation process is very hard to simulate because it varies over time. For each particular time, there is a winding curved water surface. If we overlay the water surface calculated from a certain time with DEM data, then the inundation area is where the water level is greater than topography elevation. As a result, the key point of flood inundation simulation is to calculate water surface height. According to different inundation models, there are three main computation methods: the flat-water model, 1-D hydraulic model and the 2-D hydraulic model.

The flat-water model assumes that water level is a horizontal plane. In this method, flooding of cities or coastal areas due to storms or rise of water level can be modeled relatively easily (Demirkesen et al., 2007; Wang et al., 2002; John, 2001). Two common methods are used to decide the inundation extent from DEM: the bathtub approach (Moorhead and Brinson, 1995; Titus and Richman, 2001) and the seeded region growing approach (Poulter et al., 2008).

The Bathtub approach, also called "zero-side rule", does not take connectivity issue of DEM grid cells into consideration. All the DEM grid cells whose elevation values are below floodwater level are regarded as flooded areas, and the inundation extent consisted of DEM grid coverage, as expressed by Eq. (4):

$$\text{Flood Extent} = \{\text{cell}: Z_{\text{cell}} < Z_{\text{water level}}, \text{cell} \in Q\} \tag{4}$$

where Z_{cell} is the elevation value of DEM grid cell, $Z_{\text{water level}}$ fixes the level of floodwater, and Q is the assemblage of DEM grid cells.

The seeded region growing approach considers DEM grid cell connectivity. The premise of the inundation of DEM grid cells is that the elevation is below the floodwater level and also next to an inundated DEM grid cell. This approach usually chooses some inundated DEM grid cells as seeds and then simulates the flood diffusion by four-side or eight-side rule. The flood extent consists of the coverage of DEM grid, as expressed by Eq. (5):

$$\text{Flood Extent} = \{\text{cell}: Z_{\text{cell}} < Z_{\text{water level}} \wedge \text{cell connect with point, cell} \in Q, \text{point} \in P, P \subseteq Q\} \quad (5)$$

where Z_{cell} is the elevation value of DEM grid cell, $Z_{\text{water level}}$ fixes the level of floodwater, point is a real inundated seeded grid cell, Q is the assemblage of DEM grid cells, and P is the assemblage of inundated seeded grid cells among the whole DEM grid.

1-D hydraulic models can divide watercourses into cross sections and get the information of the water level and flow of cross sections for unique time points. Because 1-D hydraulic models do not involve detailed topography information, it is hard to extract the parameters of inundation simply through calculating the water level of cross sections. A good way to solve the problem is to calculate the actual depth of every DEM grid cell and then decide the inundation extent (Tate et al., 1999). Similar to the flat-water model, this model has to solve the connectivity issue during the process of performing interpolation on DEM grid cells that are in-between cross sections. Interpolated cells that are not inundated cannot be connected with the real inundated DEM grid cells of the watercourse. Previous work suggests that this issue can be solved using methods such as geostatistical interpolation routines (March et al., 1990; Sorensen et al., 1996), neighbourhood analysis (Jonge et al., 1996), and cost distance mapping (Werner, 2001).

2-D hydraulic models, two common modeling computational meshes are regular tessellation and triangular irregular net-TIN. Triangular irregular net-TIN is more popular has an advantage on showing the topographic reliefs because it can improve the density of some areas of the triangular mesh to adjust to the changes of terrain and provide a better realization of topographic relief (Casas et al., 2006). According to different solutions of hydraulic computational equations, this model can get the water level of every mesh node or the central point of mesh element at different time. As the hydraulic computation mesh is an approximate expression of digital terrain, flood water level and inundation depth of each mesh unit can be derived after calculating every water level value. Floodplain extent and inundation depth can be calculated directly if there is low demand for result precision (Marks et al., 2000).

3.2 Local inverse distance weighted interpolation

With high-resolution DEM data, it is not precise to give the floodwater level for the whole DEM grid cells in the mesh element directly because the actual elevation value of each cell in the DEM grid is different. One reasonable way is to calculate water level of every DEM grid cell through spatial interpolation technology like 1-D hydraulic modeling. Inverse distance weighted interpolation is a comparatively simple way to get the spatial interpolation data, which can interpolate the value of unknown points with given the location and value of known points. The common equation of inverse distance weighted interpolation is as follows:

$$z(x_j) = \frac{\sum_{i=1}^{n} z(x_i) \cdot d_{ij}^{-r}}{\sum_{i=1}^{n} d_{ij}^{-r}} \tag{6}$$

In this equation, x_j stands for the unknown points that need to be interpolated, $z(x_i)$ is the elevation of No.i known point x_i, d_{ij}^{-r} is the distance between each pair of unknown and known points. Usually, r is set as 2 for spatial data interpolation. In a high-resolution DEM, we could get a water level value for each central point of every DEM grid cell through interpolation based on the equation above, and compare the water level value with the elevation value of DEM grid cell. If the water level value is higher than that of the DEM grid cell, it means this grid cell is inundated. The inundation depth of the DEM grid cell is the water level value minus the grid cell elevation value.

It is of high importance to choose computational mesh nodes as the known interpolated points for the water level interpolation of DEM grid cells because it is improper to get all the nodes in a hydraulic model involved in water level interpolation when tens or even hundreds of thousands computational mesh nodes are involved. Figure 5 shows a non-structural modeling computation mesh (TIN). The computational water level value of the model could be located on the central point of every triangle (as C1–C13 shows) or on the node of the triangle (as P1–P12 shows) according to different solutions of the equation. For the cell located at row I and column J of the DEM grid, we can decide the location of the cell by the spatial coordinate of the central point. If a DEM grid cell (the black square) is inside P1P2P3, the following methods can be used to choose the nodes of water level interpolation:

1. The case is that the computational water level value locates at the center of the triangle. Firstly, get the coordinate and its water level value of the central point C13 of P1P2P3. Then search all the triangles that share the nodes P1, P2 and P3 with P1P2P3, and calculate the coordinate of the central points of these triangles (C1–C12) and their water level values. The Equation of water level of grid cell at row *I* and column *J* is expressed as:

$$z(x) = \frac{\sum_{i=1}^{13} z(C_i) \cdot d_{ix}^{-2}}{\sum_{i=1}^{13} d_{ix}^{-2}} \tag{7}$$

In this equation, x stands for the central point which is located at row *I* and column *J* of DEM grid, $z(C_i)$ is the water level value of No.i known point, C is the central point of the triangle, and the distance between each pair of No.i known point and grid node x is represented by d_{ix} raised to the power r, which is set as 2 for spatial data interpolation.

2. The case is that the computational water level value is located at the node. Firstly, get the coordinate and its water level value of the nodes P1, P2 and P3 of P1P2P3. Then search all the triangles that share the nodes P1, P2 and P3 with P1P2P3, and calculate the coordinate of all the nodes of these triangles (P4–P12) and their water level values. The Equation of water level of grid cell at row I and column J is expressed as:

$$z(x) = \frac{\sum_{i=1}^{12} z(P_i) \cdot d_{ix}^{-2}}{\sum_{i=1}^{12} d_{ix}^{-2}} \tag{8}$$

In this equation, x stands for the central point which is located at row I and column J of DEM grid, $z(x)$ is the water level elevation of x, $z(P_i)$ is the water level value of No.i known point, P is the vertex of the triangle, and the distance between each pair of No.i known point and grid node x is represented by d_{ix} raised to the power r, which is set as 2 for spatial data interpolation.

The method mentioned above can interpolate the inside of actual flood extent. As the water level elevation of all the known points that are calculated in local areas are equal to the DEM grid cell elevation, DEM grid cells that are not inundated can be decided without interpolating, which reduces the amount of calculation. The method can also be employed for other kinds of computational grid, like a quadrilateral grid.

3.3 Inundated grid cells storing and labelling

Because much micro-topography information is retained in high-resolution LiDAR-derived DEM data, many man-made surface features become a part of the DEM, like dams and trenches and the surfaces of ponds that cannot be represented on some mid- or low-resolution DEM (Fig. 6). Suppose that there is a pond surrounded by levees in four-sides. Although the pond becomes inundated during the process of interpolation, it is not actually flooded because the levees do not suffer from the flood. This is a typical false inundation area. Another issue is ringed mountains, although the elevation of some areas among mountains is lower than flood water level, these areas are not flooded because of the protection of the mountains.

To solve the problem, calculated the actual flood extent based on the connectivity principle. However, some judgment methods to solve the connectivity problem of flat-water and 1-D hydraulic models are based on the entire DEM. These methods cannot be applied to high-resolution DEM data because of the prohibitive DEM size and the computation capability required. Using the seeded region growing method, a difficult amount of data to process, 8.36 GB (220 000 Rows × 51 000 Columns × 8 Bytes ≈ 8.36 GB), stored in the memory of a computer is required when dealing with the DEM data of our study area. On the other hand, the seeded region growing method is a recursive algorithm with low efficiency of computation. Problems like recursion might be too deep when dealing with a large amount of data and the stack of a computer is overflowed to the extent that computation failures can occur. As a result, it is not an idealistic way to employ such neighborhood analysis methods to solve DEM grid connectivity problems when facing a large scale, high resolution, and an enormous amount of DEM data.

Due to a large amount of DEM data, which is hard to read for one time, it is better to divide the data into strips to read. As Fig. 7 shows, DEM data is divided into 5 strips spatially with each being read at one time. The results of water level interpolations are concurrently stored on a raster file with a null value grid equal to the source DEM data. Every time individual strip water level is interpolated, the result is stored on a corresponding raster file. To process large volumes of DEM data, the memory that has been taken up by the previous strip is released before next data strip is read.

There are two states for every grid cell during DEM grid interpolation: un-inundated and might-be-inundated. This is typical binary raster data. If we perform run-length compressed encoding to the sequential might-be-inundated DEM grid cells in raster rows, we can mark all the might-be-inundated cells and store them in memory. Run-length encoding is a typical compressed method for raster data (Chang et al., 2006; He et al., 2011), which encodes the cells with same value in compression. Every run-length only needs to mark the cells where it starts across where it ends, which reduces the storage of data remarkably. Figure 7 shows the run-length compressed encoding of the might-be-inundated DEM grid cells. Area A in blue is the real inundation extent where there are three islands. There is a false inundation area inside the middle island. The following are the equations of run-length data and run-length list on the raster:

$$\text{Run Length Dataset} = \{\text{RLList}:\text{RLList} = (\text{RowIndex}, \text{RLNum}, \text{RLS})\} \tag{9}$$

$$\text{RLS} = \{\text{RL}:\text{RL} = (\text{RLIndex}, \text{StartCol}, \text{EndCol})\} \tag{10}$$

As Eq. (9) shows, run-length data is mainly comprised of the RL Lists on every raster row. The list means the run-lengths of current raster rows, on which there are RowIndex, RLNum and RLS. In Eq. (10), RLS consists of all the run-lengths on one raster row, and each run-length carries its RLIndex, StartCol and EndCol.

3.4 Connectivity detection principle

After finishing DEM grid water level interpolation and storage of run-length compressed encoding of inundated cells, the connectivity issue of DEM grid cells can be solved by run-length boundary tracing technology (Quek, 2000). To prove the connectivity of two inundated cells of DEM randomly, only the judgment of connectivity of the corresponding run-lengths is needed. Both the right and left borders of a run-length are traced vertically and horizontally. if the two run-lengths are connected, then their borders can be traced to form a closed loop.

As Fig. 8 shows, three inundated cells in a raster field are marked in purple. To prove the connectivity between Inundated cell 1 and Inundated cell 3 the run-length of

HESSD
12, 2011–2046, 2015

Title Page
Abstract Introduction
Conclusions References
Tables Figures
◂◂ ▸▸
◂ ▸
Back Close
Full Screen / Esc
Printer-friendly Version
Interactive Discussion

Inundated cell 1 (the first run-length on the raster row) and Inundated cell 3 (the fourth run-length on the raster row) must be found. If these run-lengths are connected the boundary trace from the left of the run-length of 1 (as is shown from the graph) to the right of 3 as long as it is on the left of 1.

If the boundary trace from the left of the run-length of Inundated cell 1 meets the right of the run-length of Inundated cell 3, then the cells can be connected. Likewise, if the run-length of 1 and the run-length of 2 cannot meet each other by boundary tracing, then they are not connected. Based on mutual exclusion, as long as we know that 1 is the real inundation area, all the areas connected to 1 are real inundation areas, and all the areas connected to 2 are false inundation areas. As a result, the run-lengths have already carried the information of connectivity between inundation grid cells and the connectivity problem could be worked out through boundary tracing. Compared with the seeded region growing method, this method only need search along the run-length borders to prove the connectivity between cells, allowing for far faster computation speed.

3.5 False inundation area exclusion

Based on the method mentioned above, we can remove false inundation areas from run-length boundary tracing and get the map of flood extent and depth. Figure 9-(1) shows the run-length boundary tracing and flood extent, in which run-lengths is marked in red rectangles. DEM data only includes 25 raster rows, the model computation mesh is only expressed by four triangles, and the run-lengths are simplified. The water level value of the central point of the mesh element is calculated by model computation, so we can calculate the flood extent by tracing the boundaries of the run-lengths, which can be searched on the central points of the whole computational model elements.

Take Fig. 9-(1) for example, the inundated central point of ABC can be found on the first run-length on the eleventh raster through its spatial coordinate. From the left of this run-length, the outer boundary of flood extent can be traced (Fig. 9-(1)) and from the right of this run-length, one of the inner boundaries of flood extent can be traced

HESSD
12, 2011–2046, 2015

(Fig. 9-(2)). The outer boundary of the entire flood extent can be also traced through boundary tracing of the run-length that can be searched from the central point of CDE (the 9th row). To avoid repetition of run-length tracing, and to mark real inundated run-lengths, it is important to set two labels along two sides of the run-length to indicate whether a run-length has previously been traced. Run-lengths are marked as traced once one of the sides is traced. Boundary tracing of the run-length where the central point of CDE is located is not performed when the run-length of the central point of ABC has been traced.

After boundary tracing through all the central points of the inundated computational mesh elements, some of the run-lengths are only traced by one side, like rows 5–8 and 12–17 in Fig. 9-(2). They are located at the islands of the flood extent. Traverse through the run-lengths to search the islands of the flood extent. Once one side of a run-length is traced while the other not, all the islands can be found by tracing from the untraced side and performing boundary tracing (Fig. 9-(3)). At this time, there are only two kinds of run-length. One is that each side of the run-length is traced, and the other is that neither side of the run-length is traced. The extent of untraced run-lengths shows false inundation areas. Therefore, the false inundation extent can be automatically removed by boundary tracing. Meanwhile, flood extent and depth can be interpolated automatically from the traced run-length (Fig. 9-(4)).

4 Results and discussion

4.1 Flood inundation results

According to the principle mentioned above, we get the 50 periods' flood extent and depth of Gongshuangcha Polder of Dongting Lake area. Figure 10 (No.10, No.30 and No.50 periods) shows the comparison between the result from the 2-D hydraulic model and the result of the method mentioned above. The resolution of the 2-D hydraulic model mesh is above 100 m, whereas this method mentioned above interpolates the water level through 1 m high-resolution DEM. As a result, although the whole flood extents differ little, the distributions of flood depth are very different from each other. The maximum inundation depth calculated by our method is 70 cm higher than that of the 2-D hydraulic model.

Figure 11 shows the No.50 period of process of inundation and its regional enlarged view. Figure 11-(1) is the high-resolution aerial remote sensing image taken by an airborne LiDAR system, whose spatial resolution is 0.3 m. From this image we can see the distribution of farmlands, roads, channels, levees and houses clearly, among which the houses are constructed along rivers and levees. Figure 11-(2) and 11-(3) are the 2-D hydraulic model and our methods regional enlarged view of the inundation area. The mesh resolution of a 2-D hydraulic model is coarser compared with the geographic features of roads and houses, so the result can only prove that the flood depth of that area is lower while the ponds on the left of the image cannot be expressed. It also cannot show the flood condition of every house. However, with the help of our method, important geographic features can be clearly expressed. From Fig. 11-(3) it is obvious that not only the flood condition of channels, ponds and levees are clearly expressed, but also the difference of flood depths between ridges of paddy fields. In Fig. 11-(3) there are three linear areas which are not inundated. From Fig. 11-(4) we can tell that those are levee crests on which houses and roads are being constructed.

4.2 Inundation area and volume statistics

We compare the flood extents calculated from the 2-D hydraulic model and the method mentioned above for 50 different periods. In the 2-D hydraulic model, the flood extent is calculated by adding up every inundated triangle's area from the hydraulic computational mesh, while in the method of this paper, the flood extent is calculated by summing every real inundated cell area based on of 1 m-resolution DEM data. It can be expected that the flood extent calculated from the 2-D hydraulic model is larger than that from the method of this paper (Fig. 12). The 2-D hydraulic model cannot take the micro-topography information into full consideration, and many details cannot be shown on

HESSD
12, 2011–2046, 2015

the model computational mesh, like some secondary levees, ponds and steep slopes. We get a smaller area result because we can get rid of the parts in the computational mesh whose elevation values are higher than the interpolated water levels.

Among the 50 periods, the flood area calculated by a 2-D hydraulic model surpasses that of our method by 5–17 %.The exceeding flood area is getting larger. In the 50th period, the flood area of the 2-D hydraulic model is 6 square kilometers larger than that of this paper's method.

As for the inundation volume, the result calculated by the 2-D hydraulic model is smaller than that calculated by our method (Fig. 13). According to the previous graphs the maximum inundation depth and the regional inundation depth calculated by our method are larger than the 2-D hydraulic model, which means that the whole digital topography could be higher if we employ model computational mesh to express the topography directly. The difference of results is from 3 to 8 %, and in the 50th time-period, the inundation volume difference is 9.689×10^6 m^3.

4.3 Discussion

The precision of digital topography is a key factor for flood simulation and analysis. Spatial resolution and Vertical precision are both important for mapping of flood extent and depth. Employing high-resolution topography data can make up for the errors of a 2-D hydraulic model.

With high-resolution topography data, flood simulation can be analyzed from the basis of topography to geographic elements because some of the most important micro-topography information is accounted for by digital topography data, especially that of levees, ponds and man-made architectures. Once we take the factors from the flood extent and depth map into consideration, we can get the results with more precision.

However, a coin has two sides. With more man-made architectures using high-resolution digital topography, new problems might occur because some false topography information might be involved. For example, the airborne LiDAR point cloud data could not be distinguished from the data of channels, bridges over reaches or viaducts

HESSD
12, 2011–2046, 2015

over roads. The redundant information could affect the simulation and analysis of floodplain flow model. To remove redundant information, much later treatments are needed and might complicate the situation.

5 Conclusions

With the help of photogrammetry and remote sensing technology, we can survey the digital terrain of a large scale of reaches with high precision. Problems like a loss of topography materials and lack of data accuracy are being gradually solved, allowing for progressively greater precision for analysis and assessment of flood disaster risks. The rapid development of LiDAR technology has especially promoted the acquirement and update of digital terrain data and shown its great potential for relevant study and application to flood disaster studies.

To employ LiDAR-derived DEM to simulate flood routing directly is not realistic because of the complexity of calculation of a hydraulic model with a prohibitively high-resolution mesh. Thus, we need to construct a relative coarse model mesh on the basis of high-resolution digital topography. However, lots of micro-topography information of high-resolution DEM has been ignored when we deal with flood parameters, which have direct relation to inundation extent and depth. As a result, this paper hopes to offer a method, which integrates a 2-D hydraulic model with high-resolution LiDAR-derived DEM to simulate floodplain flow. This method can calculate the flood extent and depth with much more precision during floodplain flow modeling. With this kind of digital topography and data of residential houses and public infrastructure, the floods caused by different reasons can be analyzed in greater detail. These factors demonstrate the great application potential of our method for predictive flood simulation and accurate assessment of potential loss from flooding events.

References

Apel, H., Aronica, G. T., Kreibich, H., and Thieken, A. H.: Flood risk analyses-how detailed do we need to be?, Nat. Hazards, 49, 79–98, 2009.

Archambeau, P., Dewals, B., Erpicum, S., Detrembleur, S., and Pirotton, M.: New trends in flood risk analysis: working with 2D flow model, laser DEM and a GIS environment: Proceedings of the 2nd International Conference on Fluvial Hydraulics: River Flow 2004, 23–25 June 2004, Napoli, Italy. A.A. Balkema Publ, Leiden, the Netherlands, 2, 1395–1401, 2004.

Bates, P. D. and Anderson, M. G.: A preliminary investigation into the impact of initial conditions on flood inundation predictions using a time/space distributed sensitivity analysis, Catena, 26, 115–134, 1996.

Bates, P. D. and De Roo., A. P. J.: A simple raster-based model for flood inundation simulation, J. Hydrol., 236, 54–77, 2000.

Casas, A., Benito, G., Thorndycraft, V. R., and Rico, M.: The topographic data source of digital terrain models as a key element in the accuracy of hydraulic flood modelling, Earth Surf. Proc. Land., 31, 444–456, 2006.

Chang, C. C., Lin, C. Y., and Wang, Y. Z.: New image steganographic methods using run-length approach, Inf. Science, 176, 3393–3408, 2006.

Chen, J., Hill, A. A., and Urbano, L. D.: A GIS-based model for urban flood inundation, J. Hydrol., 373, 184–192, 2009.

CWRC: Comprehensive Treatment Planning of Dongting Lake Area, Changjiang Water Resources Commission, Wuhan, China, 2008.

Demirkesen, A. C., Evrendilek, F., Berberoglu, S., and Kilic, S.: Coastal flood risk analysis using Landsat-7 ETM+ imagery and SRTM DEM: a case study of Izmir, Turkey, Environ. Monit. Assess., 131, 293–300, 2008.

Dobosiewicz, J.: Application of digital elevation models and geographic information systems to coastal flood studies along the shoreline of Raritan Bay, New Jersey, Environ. Eng. Geosci., 8, 11–20, 2001.

Fewtrell, T. J., Duncan, A., Sampson, C. C., Neal, J. C., and Bates, P. D.: Benchmarking urban flood models of varying complexity and scale using high resolution terrestrial LiDAR data, Phys. Chem. Earth, 36, 281–291, 2011.

French, J. R.: Airborne LiDAR in support of geomophological and hydraulic modelling, Earth Surf. Proc. Land., 28, 321–335, 2003.

HESSD

12, 2011–2046, 2015

Integration of 2-D hydraulic model and high-resolution LiDAR-derived DEM

D. Shen et al.

Title Page
Abstract Introduction
Conclusions References
Tables Figures
◄ ►
Back Close
Full Screen / Esc
Printer-friendly Version
Interactive Discussion

Garcia, S. G.: GRASS GIS-embedded decision support framework for flood simulation and forecasting, Trans. GIS, 8, 245–254, 2004.
Garrote, L. and Bras, R. L.: A distributed model for real-time flood forecasting using digital elevation models, J. Hydrol., 167, 279–306, 1995.
Gichamo, T. Z., Popescu, I., Jonoski, A., and Solomatine, D.: River cross-section extraction from the ASTER global DEM for flood modeling, Environ. Modell. Softw., 31, 37–46, 2012.
Haile, A. T.: Integrating Hydrodynamic Models and High Resolution DEM(LiDAR) for flood modelling, M.S. thesis, International Institute for Geo-Information Science and Earth Observation Enschede, the Netherlands, 2005.
He, Z., Sun, W., Lu, W., and Lu, H.: Digital image splicing detection based on approximate run length, Pattern Recogn. Lett., 32, 1591–1597, 2011.
Horritt, M. S. and Bates, P. D.: Effects of spatial resolution on a raster based model of flood flow, J. Hydrol., 253, 239–249, 2001.
Jonge, T. de, Kok, M., and Hogeweg, M.: Modelling floods and damage assessment using GIS, in: HydroGIS96: Application of Geographical Information Systems in Hydrology and Water Resources Management and Planning: Proceedings of the Vienna Conference, 16–19 April 1996, IAHS Publ., 235, 299–306, 1996.
Li, J. and Wong, D. W. S.: Effects of DEM sources on hydrologic application, Comput. Environ. Urban Syst., 34, 251–261, 2010.
March, C., Lessard, G., and Gharbi, B. El.: Kriging technique for river flood representation, J. Hydraul. Res., 28, 629–643, 1990.
Marks, K. and Bates, P.: Integration of high-resolution topographic data with floodplain flow models, Hydrol. Process., 14, 2109–2122, 2000.
Merwade, V., Cook, A., and Coonrod, J.: GIS techniques for creating river terrain models for hydrodynamic modeling and flood inundation mapping, Environ. Model. Softw., 23, 1300–1311, 2008.
Moorhead, K. K. and Brinson, M. M.: Response of wetlands to rising sea level in the lower coastal plain of North Carolina, Ecol. Appl., 5, 261–271, 1995.
MWR: Report on the Feasibility of the Flood Control Project of Qianliang Lake, Gongshuangcha and East Datong Lake of Dongting Lake Areas, Ministry of Water Resources, Beijing, China, 2009.
Poulter, B. and Halpin, P. N.: Raster modelling of coastal flooding from sea-level rise, Int. J. Geogr. Inform. Sci., 22, 167–182, 2008.

HESSD
12, 2011–2046, 2015

Quek, F. K. H.: An algorithm for the rapid computation of boundaries of run-length encoded regions, Pattern Recogn., 33, 1637–1649, 2000.
Raber, G. T., Jensen, J. R., Hodgson, M. E., Tullis, J. A., Davis, B. A., and Berglund, J.: Impact of lidar nominal post-spacing on DEM accuracy and flood zone delineation, Photogramm. Engin. Remote Sens., 73, 793–804, 2007.
Samuels, P. G.: Cross section location in one-dimensional models, in: International Conference on River Flood Hydraulics, edited by: White, W. R., Wiley, Chichester, 339–350, 1990.
Sanders, B. F.: Evaluation of on-line DEMs for flood inundation modeling, Adv. Water Resour., 30, 1831–1843, 2007.
Sanyal, J. and Lu, X. X.: GIS-based flood hazard mapping at different administrative scales: a case study in Gangetic West Bengal, India, Singapore J. Trop. Geogr., 27, 207–220, 2006.
Schumann, G., Matgen, P., Cutler, M. E. J., Black, A., Hoffmann, L., and Pfister, L.: Comparison of remotely sensed water stages from LiDAR, topographic contours and SRTM, ISPRS J. Photogramm., 63, 283–296, 2008.
Sorensen, H. R., Kjelds, J. T., Deckers, F., and Waardenburg, F.: Application of GIS in hydrological and hydraulic modelling: DLIS and MIKE II-GIS, HydroGIS 96: Application of Geographical Information Systems in Hydrology and Water Resources Management and Planning: Proceedings of the Vienna Conference, 16–19 April 1996, IAHS Publ., 235, 149–156, 1996.
Tate, E. and Maidment, D.: Floodplain mapping using HEC-RAS and ArcView GIS, CRWR Online Report 99-1, Center for Research in Water Resources, University of Texas at Austin, 1999.
Titus, J. G. and Richman, C.: Maps of lands vulnerable to sea level rise: modeled elevations along the US Atlantic and Gulf coasts, Clim. Res., 18, 205–228, 2001.
Wang, Y., Colby, J. D., and Mulcahy, K. A.: An efficient method for mapping flood extent in a costal floodplain using Landsat TM and DEM data, Int. J. Remote Sens., 23, 3681–3696, 2002.
Werner, M. G. F.: Impact of grid size in GIS based flood extent mapping using a 1D flow model, Phys. Chem. Earth B, 26, 517–522, 2001.
Zerger, A.: Examining GIS decision utility for natural hazard risk modeling, Environ. Model. Softw., 17, 287–294, 2002.

HESSD
12, 2011–2046, 2015

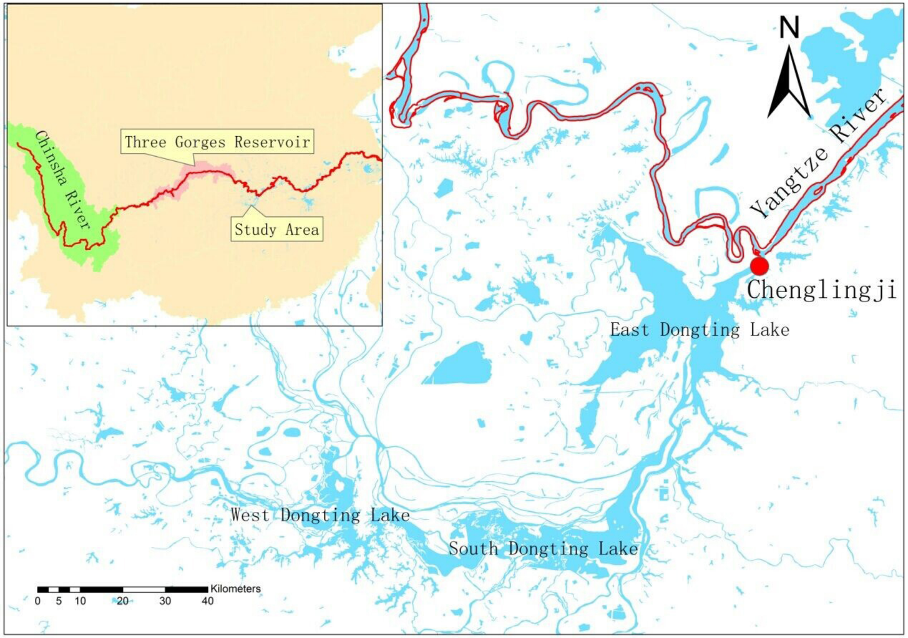

Figure 1. The location of Dongting Lake in Yangtze River Basin.

HESSD
12, 2011–2046, 2015

Integration of 2-D hydraulic model and high-resolution LiDAR-derived DEM

D. Shen et al.

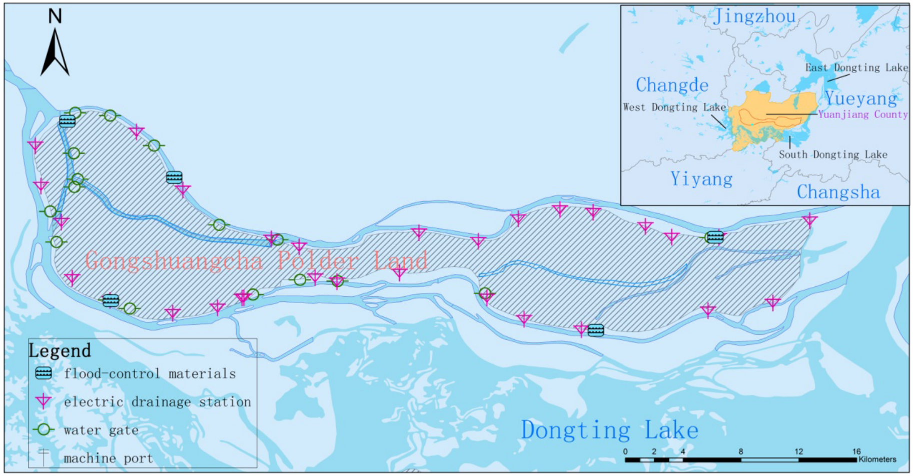

Figure 2. The location of Gongshuangcha Polder in Dongting Lake Area.

HESSD
12, 2011–2046, 2015

Integration of 2-D hydraulic model and high-resolution LiDAR-derived DEM

D. Shen et al.

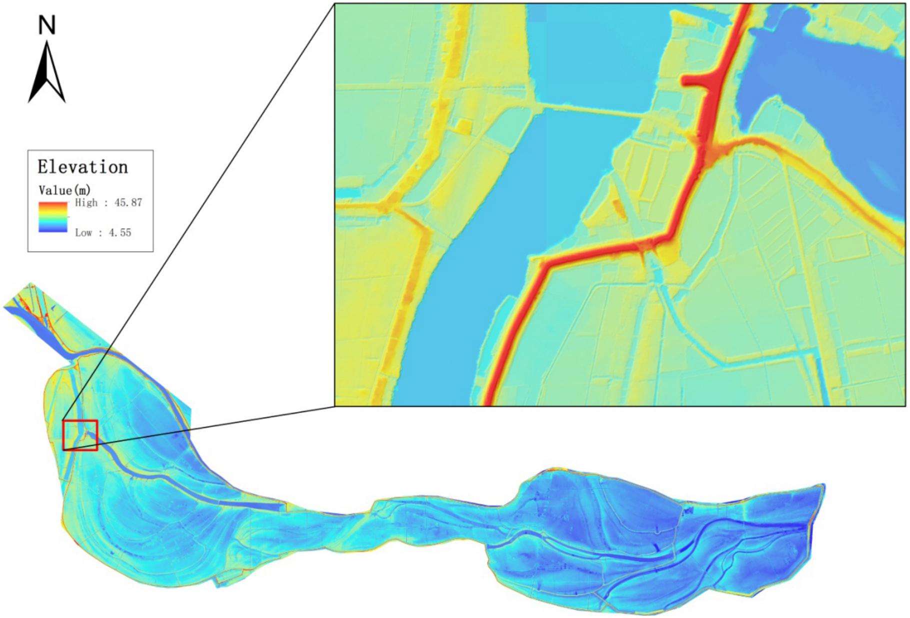

Figure 3. 1 m-resolution DEM data for the Gongshuangcha Polder. Coverage shown is 50 × 20 km, Space resolution of 1 m, DEM grid is 22 000 rows × 51 000 columns, and file size is 4.18 GB.

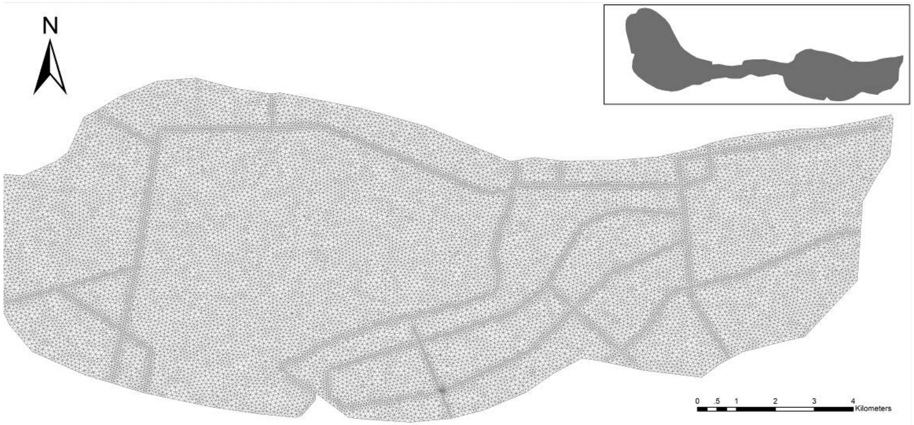

Figure 4. The 2-D hydraulic model mesh of Gongshuangcha Polder and its regional enlarged view.

HESSD
12, 2011–2046, 2015

Integration of 2-D hydraulic model and high-resolution LiDAR-derived DEM

D. Shen et al.

Title Page
Abstract Introduction
Conclusions References
Tables Figures
◀◀ ▶▶
◀ ▶
Back Close
Full Screen / Esc
Printer-friendly Version
Interactive Discussion

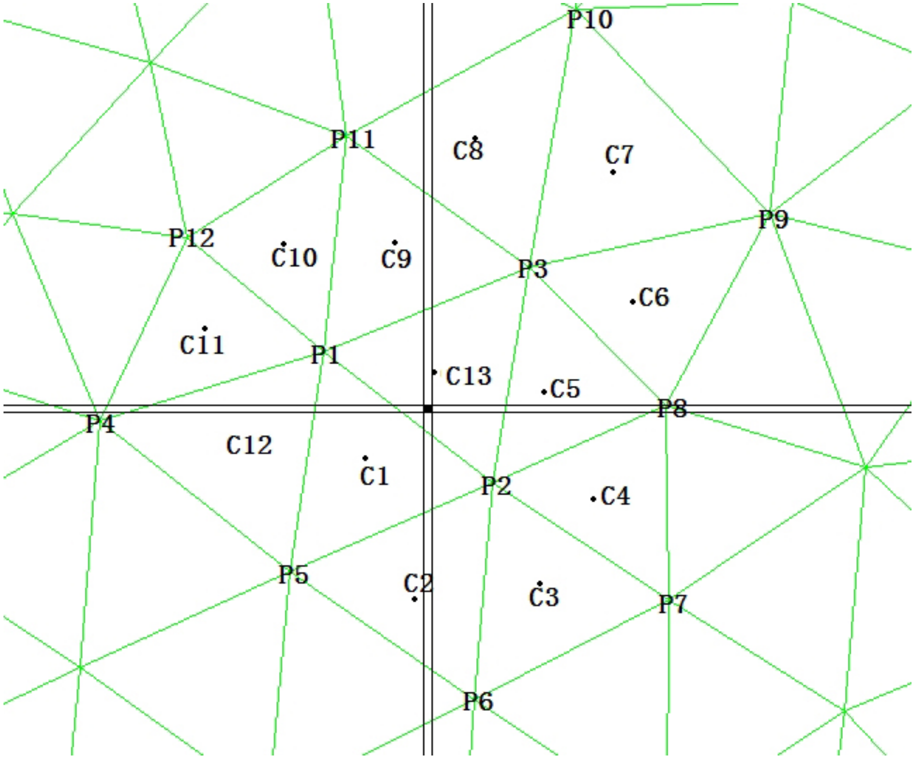

Figure 5. The scheme of spatial interpolation.

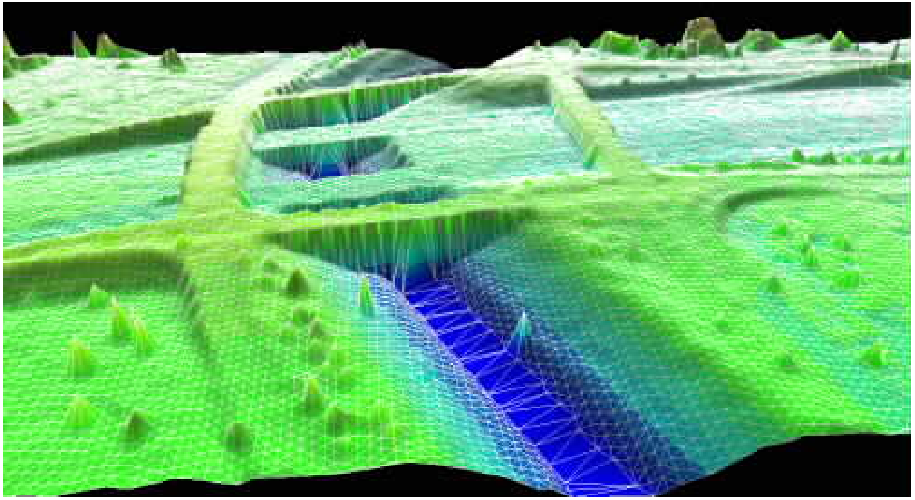

Figure 6. The micro-topography information of DEM.

HESSD
12, 2011–2046, 2015

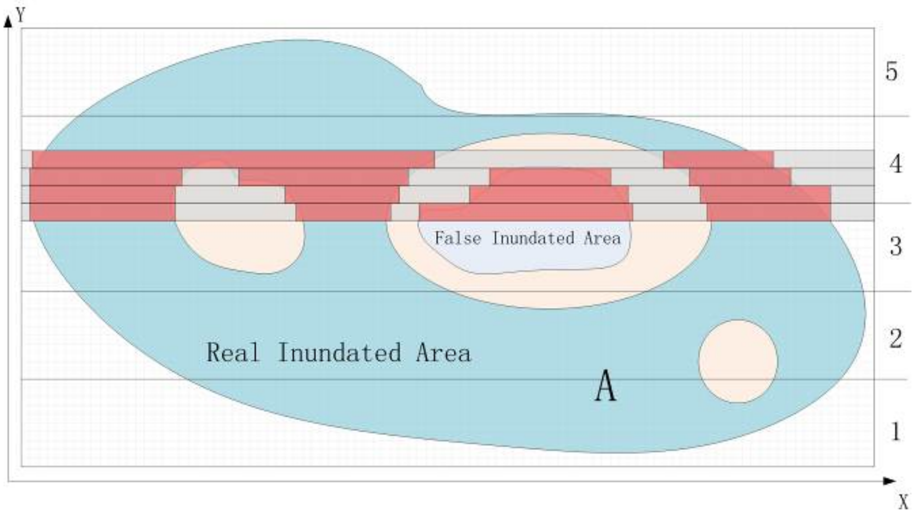

Figure 7. Run-length compressed encoding of DEM.

HESSD
12, 2011–2046, 2015

Integration of 2-D hydraulic model and high-resolution LiDAR-derived DEM

D. Shen et al.

Title Page
Abstract Introduction
Conclusions References
Tables Figures
◀ ▶
Back Close
Full Screen / Esc
Printer-friendly Version
Interactive Discussion

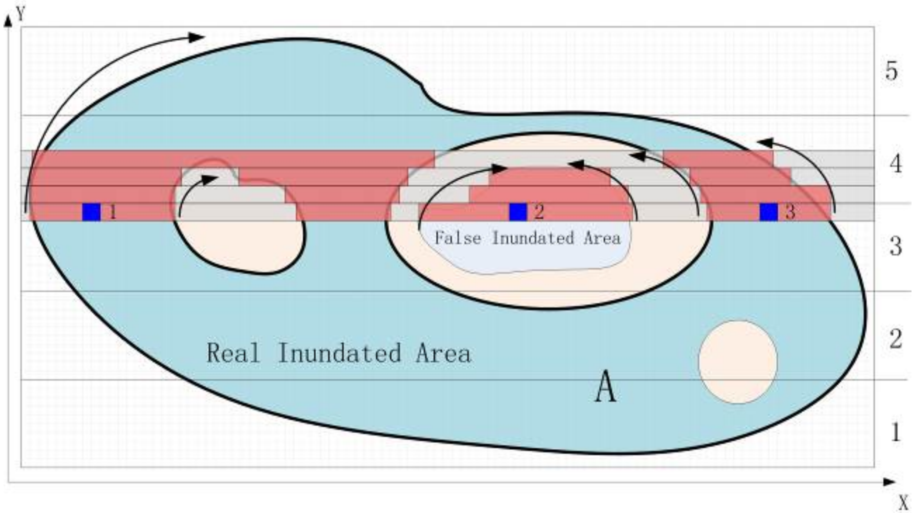

Figure 8. Connectivity detection between DEM grid cells.

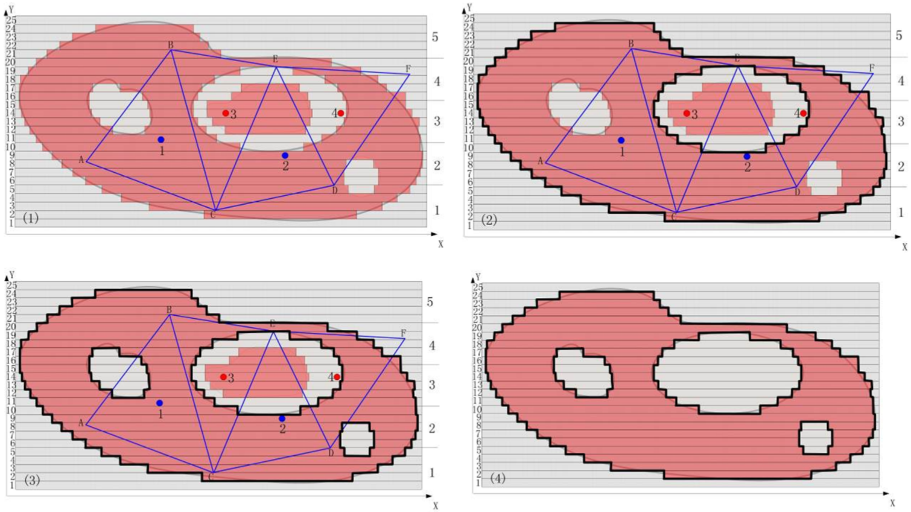

Figure 9. The scheme of run-length boundary tracing and the derived flood extent.

HESSD
12, 2011–2046, 2015

Integration of 2-D hydraulic model and high-resolution LiDAR-derived DEM

D. Shen et al.

Title Page
Abstract | Introduction
Conclusions | References
Tables | Figures
◀| |▶
◀ ▶
Back | Close
Full Screen / Esc
Printer-friendly Version
Interactive Discussion

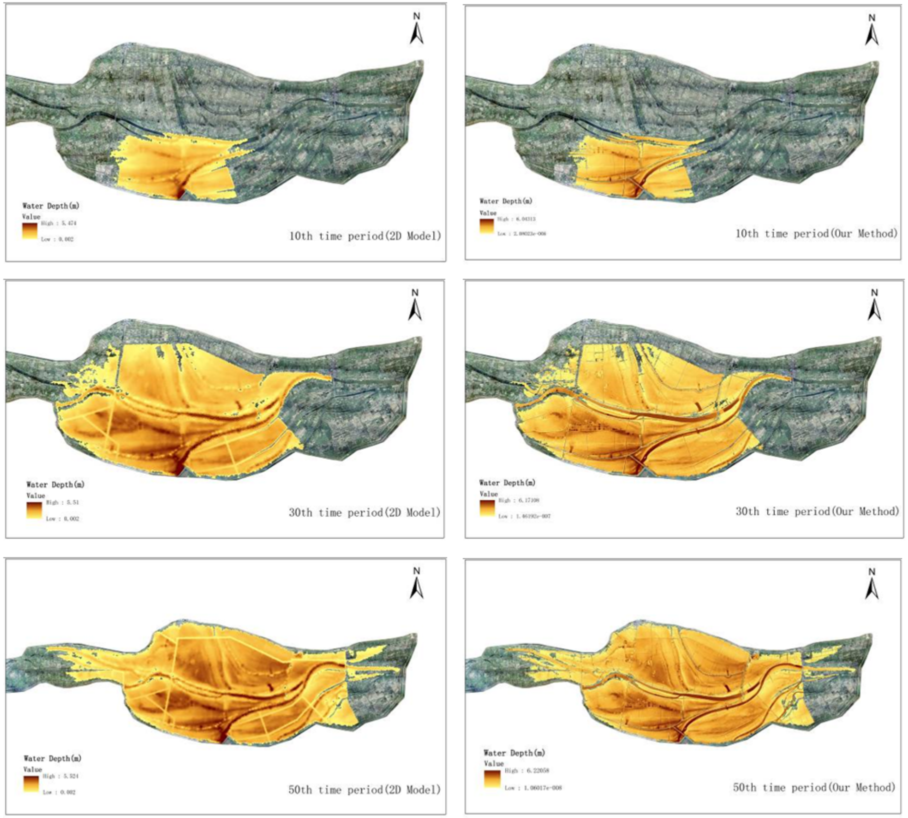

Figure 10. The scheme of the inundation process of Gongshuangcha Polder in three different time periods.

HESSD
12, 2011–2046, 2015

Integration of 2-D hydraulic model and high-resolution LiDAR-derived DEM

D. Shen et al.

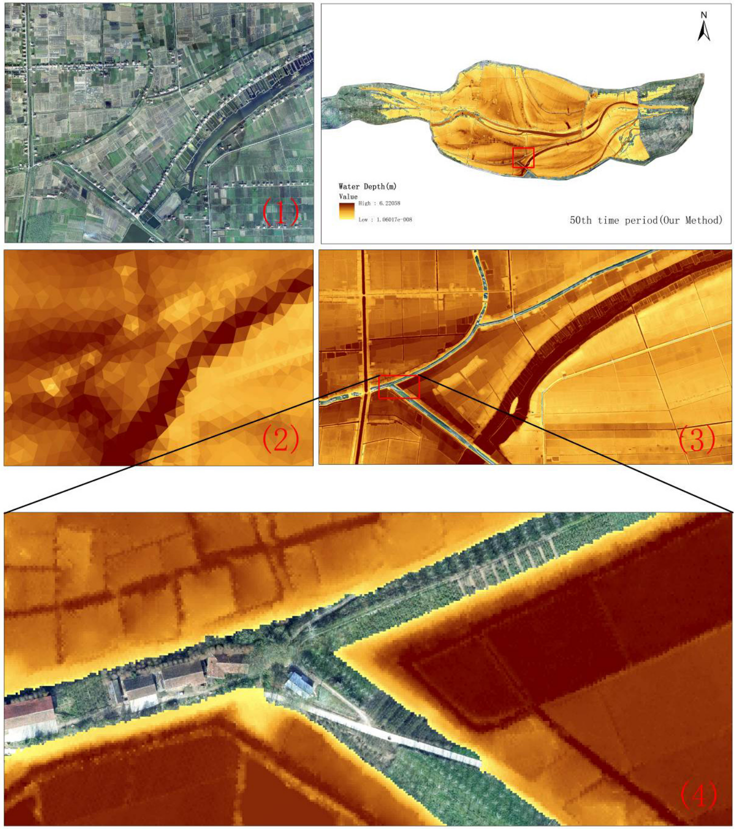

Figure 11. The scheme of the inundation process on the 50th time period and its regional enlarged view.

HESSD
12, 2011–2046, 2015

Integration of 2-D hydraulic model and high-resolution LiDAR-derived DEM

D. Shen et al.

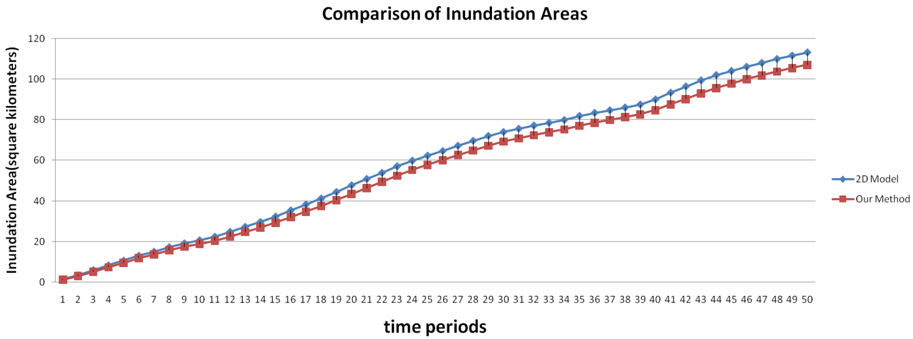

Figure 12. The comparison of inundation areas in different time periods.

HESSD
12, 2011–2046, 2015

Integration of 2-D hydraulic model and high-resolution LiDAR-derived DEM

D. Shen et al.

Title Page
Abstract Introduction
Conclusions References
Tables Figures
◀ ▶
◀ ▶
Back Close
Full Screen / Esc
Printer-friendly Version
Interactive Discussion

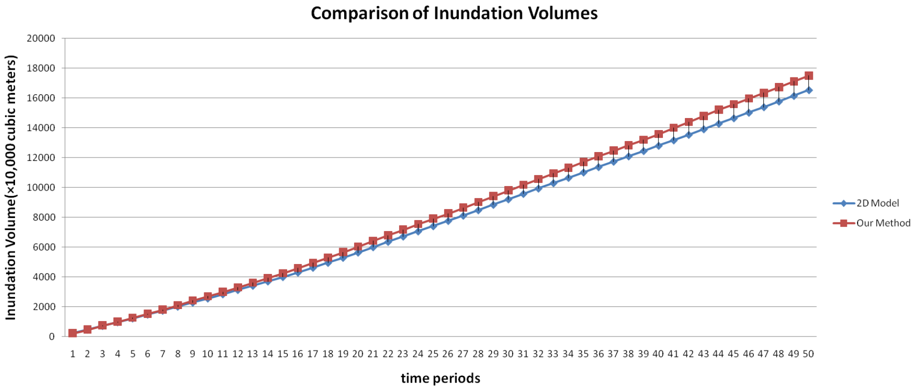

Figure 13. The comparison of inundation volumes in different time periods.

HESSD
12, 2011–2046, 2015

Integration of 2-D hydraulic model and high-resolution LiDAR-derived DEM

D. Shen et al.

Title Page
Abstract Introduction
Conclusions References
Tables Figures
◀◀ ▶▶
◀ ▶
Back Close
Full Screen / Esc
Printer-friendly Version
Interactive Discussion